Substrate-enhanced infrared near-field spectroscopy

Javier Aizpurua[1], Thomas Taubner[2,3], F. Javier García de Abajo[4], Markus Brehm[5], Rainer Hillenbrand[3,6]

[1]*Donostia International Physics Center, P. Manuel Lardizabal 4, 20018 San Sebastián, Spain*
[2]*Stanford University, 476 Lomita Mall, Stanford, CA 94305-4045, USA*
[3]*Nano-Photonics Group, Max-Planck-Institut fuer Biochemie, 82152 Martinsried, Germany*
[4]*Instituto de Óptica - CSIC, Serrano 121, 28006 Madrid, Spain*
[5]*Abteilung Molekulare Strukturbiologie, Max-Planck-Institut fuer Biochemie, 82152 Martinsried, Germany*
[6] *CIC NanoGUNE Consolider, P. Mikeletegi 56, 20009 Donostia-San Sebastián, Spain*
aizpurua@ehu.es

Abstract: We study the amplitude and phase signals detected in infrared scattering-type near field optical microscopy (s-SNOM) when probing a thin sample layer on a substrate. We theoretically describe this situation by solving the electromagnetic scattering of a dipole near a planar sample consisting of a substrate covered by thin layers. We perform calculations to describe the effect of both weakly (Si and SiO_2) and strongly (Au) reflecting substrates on the spectral s-SNOM signal of a thin PMMA layer. We theoretically predict, and experimentally confirm an enhancement effect in the polymer vibrational spectrum when placed on strongly reflecting substrates. We also calculate the scattered fields for a resonant tip-substrate interaction, obtaining a dramatic enhancement of the signal amplitude and spectroscopic contrast of the sample layer, together with a change of the spectral line shape. The enhanced contrast opens the possibility to perform ultra-sensitive near field infrared spectroscopy of monolayers and biomolecules.

OCIS codes: (180.4243) Near-field microscopy; (240.6490) Spectroscopy, surface; (290.5825) Scattering theory; (300.6340) Spectroscopy, infrared

References and links

1. Y. Inouye, and S. Kawata, "Near-field scanning optical microscope with a metallic probe tip," Opt. Lett. **19,** 159–161 (1994).
2. F. Zenhausern, Y. Martin, and H. K. Wickramasinghe, "Scanning Interferometric Apertureless Microscopy: Optical Imaging at 10 Angstrom Resolution," Science **269,** 1083–1085 (1995).
3. R. Hillenbrand, and F. Keilmann, "Complex optical constants on a subwavelength scale," Phys. Rev. Lett. **85,** 3029–3032 (2000).
4. R. Bachelot, G. Lerondel, S. Blaize, S. Aubert, A. Bruyant, P. Royer, "Probing photonic and optoelectronic structures by apertureless scanning near-field optical microscopy," Microsc. Res. Tech. **64,** 441–452 (2004).
5. N. Anderson, A. Bouhelier, and L. Novotny, "Near-field photonics: tip-enhanced microscopy and spectroscopy on the nanoscale," J. Opt. A **8,** S227–S233 (2006).
6. Z. H. Kim, and S. R. Leone, "High-resolution apertureless near-field optical imaging using gold nanosphere probes," J. Phys. Chem. B **110,** 19804–19809 (2006)
7. A. Lahrech, R. Bachelot, P. Gleyzes, and A. C. Boccara, "Infrared-reflection-mode near-field microscopy using an apertureless probe with a resolution of lambda / 600," Opt. Lett. **21,** 1315–1317 (1995).

#90017 - $15.00 USD Received 21 Nov 2007; revised 16 Jan 2008; accepted 17 Jan 2008; published 22 Jan 2008

8. B. Knoll, and F. Keilmann, "Near-field probing of vibrational absorption for chemical microscopy," Nature **399,** 134–137 (1999).
9. B. B. Akhremitchev, and G. C. Walker, "Apertureless Scanning Near-Field Infrared Microscopy of Rough Polymeric Surface," Langmuir. **17,** 2774–2781 (2001).
10. I. Kopf, J. S. Samson, G. Wollny, C. Grunwald, E. Brundermann, and M. Havenith, "Chemical imaging of microstructured self-assembled monolayers with nanometer resolution," J. Phys. Chem. C **111,** 8166–8171 (2007).
11. M.B. Raschke, L. Molina, T. Elsaesser, D.H. Kim, W. Knoll, and K. Hinrichs, "Apertureless near-field vibrational imaging of block-copolymer nanostructures with ultrahigh spatial resolution," ChemPhysChem **6**, 2197–2203 (2005).
12. A. Huber, D. Kazantsev, F. Keilmann, J. Wittborn, and R. Hillenbrand, "Simultaneous infrared material recognition and conductivity mapping by nanoscale near-field microscopy," Adv. Mater. **19,** 2209–2212 (2007).
13. T. Taubner, D. Korobkin, Y. Urzhumov, G. Shvets, and R. Hillenbrand, "Near-field Microscopy Through a SiC Superlens," Science **313,** 1595–1595 (2006).
14. A. Cvitkovic, N. Ocelic, J. Aizpurua, R. Guckenberger, and R. Hillenbrand, "Infrared Imaging of Single Nanoparticles via Strong Field Enhancement in a Scanning Nanogap," Phys. Rev. Lett. **97,** 060801 (2006).
15. A. Cvitkovic, N. Ocelic, and R. Hillenbrand, "Material-specific optical recognition of sub-10 nm particles by substrate-enhanced scattering-type near-field microscopy," Nano Lett. **7,** 3177–3181 (2007).
16. T. Taubner, R. Hillenbrand, and F. Keilmann, "Nanoscale polymer identification by spectral signature in scattering infrared near-field microscopy," Appl. Phys. Lett. **85,** 5064–5066 (2004).
17. M. Brehm, T. Taubner, R. Hillenbrand, and F. Keilmann, "Infrared Spectroscopic Mapping of Single Nanoparticles and Viruses at Nanoscale Resolution," Nanoletters **6,** 1307–1310 (2006).
18. T. Taubner, R. Hillenbrand, and F. Keilmann, "Performance of visible and mid-infrared scattering-type near-field optical microscopes," J. Microsc. **210,** 311–314 (2003).
19. J. A. Porto, P. Johansson, S. P. Apell, and T. Lopez-Rios, "Resonance shift effects in apertureless scanning near-field optical microscopy," Phys. Rev. B. **67**, 085409 (2003).
20. R. M. Roth, N. C. Panoiu, M. M. Adams, R. M. Osgood, C. C. Neacsu, and M. B. Raschke, "Resonant-plasmon field enhancement from asymmetrically illuminated conical metallic-probe tips," Opt. Express **14,** 2921–2931 (2006).
21. R. Esteban, R. Vogelgesang, and K. Kern, "Simulation of optical near and far fields of dielectric apertureless scanning probe," Nanotechnology **17,** 475–482 (2006).
22. R. Esteban, R. Vogelgesang, and K. Kern, "Tip-substrate interaction in optical near-field microscopy," Phys. Rev. B **75,** 195410 (2007).
23. F. Keilmann, and R. Hillenbrand, "Near-field optical microscopy by elastic light scattering from a tip," Phil. Trans. Roy. Soc. A **362**, 787–805 (2004).
24. V. Romanov, and G. C. Walker, "Infrared near-field detection of a narrow resonance due to molecular vibrations in a nanoparticle," Langmuir **23,** 2829–2837 (2007).
25. R. Hillenbrand, T. Taubner, and F. Keilmann, "Phonon-enhanced light-matter interaction at the nanometer scale," Nature **418,** 159–162 (2002).
26. T. Taubner, F. Keilmann, and R. Hillenbrand, "Nanomechanical resonance tuning and phase effects in optical near-field interaction," Nano Lett. **4,** 1669–1672 (2004).
27. M. B. Raschke and C. Lienau, "Apertureless near-field optical microscopy: Tip-sample coupling in elastic light scattering," Appl. Phys. Lett. **83,** 5089–5091 (2003).
28. T. Taubner, F. Keilmann, and R. Hillenbrand, "Nanoscale-resolved subsurface imaging by scattering-type near-field optical microscopy," Opt. Express **13,** 8893–8899 (2005).
29. N. Anderson, P. Anger, A. Hartschuh, and L. Novotny, "Subsurface Raman imaging with nanoscale resolution," Nano Lett. **6,** 744–749 (2006).
30. G. Y. Panasyuk, V. A. Markel, P. S. Carney, and J. C. Schotland, "Nonlinear inverse scattering and three-dimensional near-field optical imaging," Appl. Phys. Lett. **89,** 221116 (2006).
31. E.G. Bortchagovsky, and U. C. Fischer, "On the modulation of optical transmission spectra of thin dye layers by a supporting medium," J. Chem. Phys. **117,** 5384–5392 (2002).
32. S. G. Moiseev, and S. V. Sukhov, "Near-Field optical microscopy in the presence of an intermediate layer," Opt. Spectrosc. **98,** 308–313 (2005).
33. M. Brehm, "Infrarot-Mikrospektroskopie mit einem Nahfeldmikroskop," PhD. Thesis 2006, TU Mnchen, Verlag Dr. Hut, ISBN 978-3-89963-482-2.
34. N. Ocelic, A. Huber, and R. Hillenbrand, "Pseudoheterodyne detection for background-free near-field spectroscopy," App. Phys. Lett. **89,** 101124 (2006).
35. H. Weyl, "Ausbreitung elektromagnetischer Wellen uber einem ebenen Leiter," Ann. Phys. (Leipzig) **60,** 481–500 (1919).
36. G. W. Ford and W. H. Weber, "Electromagnetic interactions of molecules with metal surfaces," Phys. Rep. **113,** 195–287 (1984).
37. F. J. García de Abajo, "Light scattering by particle and hole arrays," Rev. Mod. Phys. **79,** 1267–1290 (2007).
38. E. D. Palik, "Handbook of optical constants of solids," Academic, New York, (1985).

#90017 - $15.00 USD Received 21 Nov 2007; revised 16 Jan 2008; accepted 17 Jan 2008; published 22 Jan 2008

39. U. Fano, "Effects of Configuration Interaction on Intensities and Phase Shifts," Phys. Rev. B **124,** 1866–1878 (1961).
40. B.B. Akhremitchev, Y.J. Sun, L. Stebounova, and G.C. Walker, "Monolayer-sensitive infrared imaging of DNA stripes using apertureless near-field microscopy," Langmuir **18,** 5325–5328 (2002).
41. F. Neubrech, T. Kolb, R. Lovrincic, G. Fahsold, A. Pucci, J. Aizpurua, T. W. Cornelius, M. E. Toimil-Molares, R. Neumann, and S. Karim, "Resonances of individual metal nanowires in the infrared," Appl. Phys. Lett. **89,** 253104 (2006).
42. K.R. Rodriguez, H. Tian, J.M. Heer, S. Teeters-Kennedy, and J.V. Coe, "Interaction of an infrared surface plasmon with an excited molecular vibration," J. Chem. Phys. **126,** 151101 (2007).
43. H. Wang, J. Kundu, and N. J. Halas, "Plasmonic Nanoshell Arrays Combine Surface-Enhanced Vibrational Spectroscopies on a Single Substrate," Angew. Chem. **46,** 9040–9044 (2007).
44. A. V. Zayats, "Electromagnetic field enhancement in the context of apertureless near-field microscopy," Opt. Comm. **161,** 156–162 (1999).
45. A. Christ, Y. Ekinci, H. H. Solak, N. A. Gippius, S. G. Tikhodeev, and O. J. F. Martin, "Controlling the Fano interference in a plasmonic lattice," Phys. Rev. B **76,** 201405(R) (2007).
46. U. C. Fischer, "Latex Projections Patterns, in Procedures in Scanning Probe Microscopy," Editors: R.J. Colton, et al., John Wiley & Sons. 10–11 (1998).
47. T. R. Jensen, M. D. Malinsky, C. L. Haynes, and R. P. Van Duyne, "Nanosphere lithography: Tunable Localised Surface Plasmon Resonance Spectra of Silver Nanoparticles," J. Phys. Chem. B **104,** 10549–10556 (2000).
48. M.S. Anderson, "Enhanced infrared absorption with dielectric nanoparticles," Appl. Phys. Lett. **83,** 2964–2966 (2003).
49. F. Neubrech, A. Pucci, T. W. Cornelius, and S. Karim, A. Garcia-Etxarri, and J. Aizpurua, "Giant vibrational signals from molecules by the action of a tailored infrared nanoantenna," in preparation.

1. Introduction

The development of the scattering type near field optical microscopy (s-SNOM) [1, 2] as a standard tool for visible [3, 4, 5, 6] and infrared [7, 8, 9, 10, 11] microscopy and spectroscopy of nanostructures allowed for an extensive variety of applications such as mapping materials and doping concentrations in nanoelectronic circuits [12], studying superlensing [13], infrared imaging of single nanoparticles [14, 15], or vibrational polymers recognition by near-field infrared fingerprint spectroscopy [16, 17], among others. s-SNOM takes advantage of the confined electromagnetic field of a sharp metal tip for local probing of the optical properties of a sample, with a resolution of the order of 10 nm-30 nm, even at long mid-infrared wavelengths [18]. Although full electromagnetic calculations are often needed to understand quantitatively all aspects and parameters governing the near-field signals measured with s-SNOM [19, 20, 21, 14, 22], a simple model of the tip and sample coupling where the system is described as a point dipole (tip) over a semiinfinite medium (sample) has been proven to successfully describe the main features of the s-SNOM signal [23]. This approach has enabled an understanding of material contrast [18], the correct description of the spectral response of molecular vibrations [16, 24], and the resonant tip-sample interaction in the infrared [25, 26].

Although near-field microscopy is commonly known to be surface-sensitive, it has been found that the contrast depends on the vertical composition of the sample [27]. Due to the finite penetration of the near-fields into the sample, nanoscale resolved subsurface imaging can be performed, providing the prospect of non-destructive analysis of buried interfaces [28, 29]. Subsurface probing is also relevant in the context of near field optical tomography that could lead to 3D non-destructive imaging of subsurface samples [30]. For a quantitative description of the tip-sample interaction, and probing depth, a proper theory that includes the coupling between the tip and the different sample layers including the substrate is necessary.

Here we perform fully retarded calculations of dipolar near-field coupling through layered systems to investigate the amplitude and phase signals obtained in s-SNOM when probing thin sample layers on different substrates. By theoretically varying the thickness of the sample layer, and changing the dielectric response of the substrate material, we predict that certain substrates do effectively enhance the sensitivity of s-SNOM to thin sample layers. Experimental spectra of

#90017 - $15.00 USD Received 21 Nov 2007; revised 16 Jan 2008; accepted 17 Jan 2008; published 22 Jan 2008

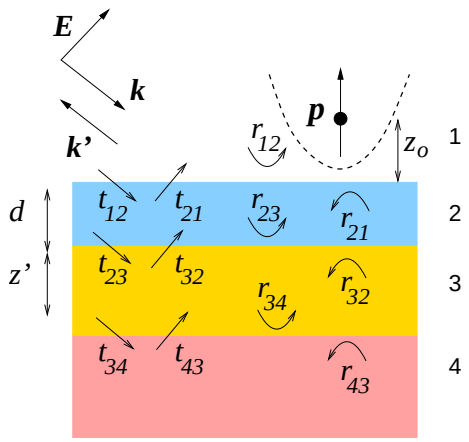

Fig. 1. Schematics of the scattering system. An induced dipole located on top of a multilayered system interacts with the incoming plane wave as well as with the layered substrate. Reflections r_{ij} and transmissions t_{ij} at each layer are labelled in the scheme. z_o is the dipole-sample separation distance, d is the thickness of the first layer (material 2=sample), and z' is the thickness of the second layer (material 3=substrate). involved in the interaction. Different media i are characterised by their local dielectric response ε_i.

a PMMA layer on different substrates confirm the predicted enhancement effect. The enhanced infrared signal amplitude and the enhanced spectral contrast of a PMMA layer in the presence of a Au substrate compared to a Si substrate leads us to propose the use of highly reflecting substrates for efficient near field optical spectroscopy of thin organic or molecular layers. We also investigate theoretically the case of resonant tip-substrate interaction and obtain an even larger enhancement of the s-SNOM signal from a thin sample layer, along with an increase of the spectral contrast, although presenting a distortion of the line shape of a single molecular absorption band [31].

2. Formalism: Dipole model for a layered system

We present in this section the electromagnetic response of a dipole above a multilayered surface [32], as a model for the light scattering produced by a s-SNOM tip on a layered material over different substrates. The scheme of the system we will address is shown in Fig. 1, where **p** denotes the interacting dipole representing the s-SNOM tip, z_o is the distance between the dipole (tip) and sample, and d and z' are the different material thickness for the sample and substrate respectively. The angle of incidence of the light is denoted by θ_{inc}, ε_i is the local dielectric response of material i, and $k = 2\pi/\lambda$ is the modulus of the wavevector. The wave vector **k**, its modulus k, and the components perpendicular k_z and parallel $Q = \sqrt{k_x^2 + k_y^2}$ to the surfaces, are defined as

$$\begin{array}{lll} k = \omega/c & k_z^i = \sqrt{k^2\varepsilon_i - Q^2} & Re\{k_z\} > 0 \\ k^i = k\sqrt{\varepsilon_i} & \mathbf{k} = (\mathbf{Q}, k_z sign(z)) & Im\{k_z\} > 0 \end{array} \tag{1}$$

with $\hbar\omega$ the energy associated with a certain wavelength λ

To calculate the fields from the dipole on top of this multilayered system, we first calculate the self-interacting dipole **p** driven by the external incoming plane wave in the presence of the

#90017 - $15.00 USD Received 21 Nov 2007; revised 16 Jan 2008; accepted 17 Jan 2008; published 22 Jan 2008

multilayered system. Once we calculate the resulting dipole, we obtain the radiation probability of this dipole considering that the radiation occurs in the presence of the layered system. In this way, we can obtain information on the amplitude s and phase φ of the radiation backscattered by the dipole. A similar approach based on an electrostatic extended dipole model, with Fresnel coefficients for the multilayers included, gives identical results [33]. Experimentally, there is additional light scattering from other parts of the tip and the sample which have to be suppressed by a pseudoheterodyne interferometric detection scheme [34] in combination with a demodulation procedure. In this technique, the tip sample-distance is modulated sinusoidally at a frequency Ω, and the signals from the detector are evaluated at the frequency $n\Omega$ with $n = 2$ or $n = 3$. Thus, theoretically demodulated n-th order amplitude s_n and phase φ_n are the magnitudes to be compared with the experiments later on.

2.1. Dipole on a surface

The dipolar moment $\mathbf{p}$ of an object with polarizability α in an external field $\mathbf{E}^0$ in the proximity of a surface can be expressed as:

$$\mathbf{p} = \alpha \mathbf{E}^0 + \alpha G \mathbf{p} \tag{2}$$

The dipole polarizability α depends on the material and shape. In our case, the dipole polarizability is assumed to be $\alpha = a^3 \frac{\varepsilon_{tip}-1}{\varepsilon_{tip}+2}$, corresponding to a sphere of radius a and dielectric response ε_{tip}. $\mathbf{E}^0$ is the external field at the dipole position (after considering the reflections and refractions at the multilayered system), and G is the dipole interaction with the multilayered system at the dipole position, produced by the dipole itself. The latter involves the response of the multilayered surface, sometimes called mirror dipole. This self-interacting dipole can be expressed as

$$\mathbf{p} = \frac{\alpha \mathbf{E}^0}{1 - \alpha G}. \tag{3}$$

The external field at the dipole $\mathbf{E}^0$ and the dipole interaction G need to be evaluated including all the reflections and transmissions of the different layers at the substrate, as depicted in the inset. These coefficients, explicitly defined in the Appendix, will be used to calculate both the external field $\mathbf{E}^0$, and the dipole interaction G in the following sections.

2.2. External field at the dipole

The external field at the point dipole E^0 is a result of the direct external field coming from the external plane wave E_d^0 plus the reflected field from the multilayered surface E_r^0:

$$E^0 = E_d^0 + E_r^0, \tag{4}$$

which can be expressed as:

$$E^0 = E_d^0 + R e^{i2k_z^{(1)} z_o} E_d^0 = (1 + R e^{i2k_z^{(1)} z_o}) E_d^0, \tag{5}$$

with R being the reflection coefficient of the entire multilayered system. The expression for this coefficient is addressed in the Appendix.

2.3. Dipole interaction

The field of the dipole is reflected by the surface and acts back on the dipole itself. Translational invariance of the surface makes it convenient to express the field of the dipole as a combination of plane waves that are reflected by the surface according to the plane-wave reflection coefficients [appendix]. This strategy was pioneered by Weyl [35] and was latter further developed

#90017 - $15.00 USD Received 21 Nov 2007; revised 16 Jan 2008; accepted 17 Jan 2008; published 22 Jan 2008

by Ford and Weber [36]. The reflected field times the dipole can be understood as a dipole-surface interaction G, which we can write as the sum (integral) over all parallel momentum components (i.e., over all plane waves into which the dipole field is decomposed). We find the following expression for the reflected field produced by the dipole itself [37]:

$$\mathbf{E}_r^{dip} = \int \frac{d^2Q}{(2\pi)^2} e^{i\mathbf{QR}} (2\pi i) \frac{1}{k_z^{(1)}} [R_s \hat{\varepsilon}_s \alpha_s^{(1)} + R_p \hat{\varepsilon}_p^- \alpha_p^{(1)-}] e^{i2k_z^{(1)} z_o}, \tag{6}$$

where

$$\hat{\varepsilon}_s = \frac{1}{Q}(-Q_y, Q_x, 0), \tag{7}$$

and

$$\hat{\varepsilon}_p^{i\pm} = \frac{1}{k^i Q}(\pm k_z Q_x, \pm k_z Q_y, -Q^2), \tag{8}$$

are unit vectors along s and p polarization directions,

$$\alpha_s = \frac{k^2}{Q}(-p_x Q_y + p_y Q_x), \tag{9}$$

and

$$\alpha_p^{i\pm} = \frac{k^2}{k^i Q}[\pm k_z (Q_x p_x + Q_y p_y) - Q^2 p_z]. \tag{10}$$

are the coefficients of such reflected waves, i is referred to the propagation medium, vacuum in this case ($i = 1$), $\mathbf{R}$ is the dipole position vector parallel to the multilayered surfaces ($\mathbf{R} = 0$ in this case), and p_x, p_y, and p_z are the components of the point dipole $\mathbf{p}$. Due to the polarization of elongated tips, being dominant in the z direction, we assume a dipole oriented only in the z direction. It is important to note that the integral of Eq. (6) extends not only over propagating plane waves ($Q < \omega/c$), but also over evanescent waves ($Q > \omega/c$). These evanescent waves can make a substantial contribution, and they are actually dominant in the non-retarded limit in which $G = e^{iQ|z-z_0|}(\varepsilon - 1)/(\varepsilon + 1)$ for a homogeneous surface.

The dipole self-interaction is then simply given by the action of the reflected field on the dipole itself, so that $G = \mathbf{p} \cdot \mathbf{E}_r^{dip}$.

2.4. Dipole radiation

Finally, the backscattered radiation can be obtained from the electromagnetic field $\mathbf{E}^d$ radiated by the self-interacting dipole $\mathbf{p}$ plus the field reflected by the multilayered surface $\mathbf{E}^r$:

$$\mathbf{E} = \mathbf{E}^d + \mathbf{E}^r = \int \frac{d^2Q}{(2\pi)^2} \frac{2\pi i}{k_z} e^{i\mathbf{QR}} \mathbf{g}, \tag{11}$$

with

$$\mathbf{g} = \mathbf{g}^d + \mathbf{g}^r, \tag{12}$$

the direct (d), and reflected (r) parts of the radiation, that are obtained as

$$\mathbf{g}^d = [\alpha_p^+ \hat{\varepsilon}_p^+ + \alpha_s \hat{\varepsilon}_s] e^{ik_z(z - z_o)} \tag{13}$$

and

$$\mathbf{g}^r = [R_p \alpha_p^- \hat{\varepsilon}_p^+ + R_s \alpha_s \hat{\varepsilon}_s] e^{ik_z(z + z_o)}], \tag{14}$$

#90017 - $15.00 USD Received 21 Nov 2007; revised 16 Jan 2008; accepted 17 Jan 2008; published 22 Jan 2008

where **R** and z are the coordinates of the far-field position vector **r** where the radiation is evaluated. The field at infinity will be given by the expression of the total field at a point $r \rightarrow \infty$, where $\mathbf{r}||\mathbf{k}$. Asymptotic analysis of the **Q** integral leads to

$$\mathbf{E} = \frac{e^{ikr}}{r}\mathbf{g}(\theta), \tag{15}$$

where we now see that g is indeed the far-field amplitude produced by the dipole and its surface reflection. From here, the intensity of the electric field at infinity per solid angle will be given by:

$$\frac{dP}{d\Omega} = |\mathbf{g}|^2, \tag{16}$$

so the probability of backscattering radiation intensity per solid angle unit is

$$\frac{dP}{d\Omega} = |g|^2 = \frac{p^2}{\varepsilon^2}k^4(1+R_p e^{i2k_z^{(1)}z_o})^2 sin^2\theta_{out}. \tag{17}$$

The phase of the scattered field can also be derived to compare with the experimental measurements of phase. In this case, the phase can be obtained as the argument of g_z, the z component of the function g. As pointed out above, in the experimental situation, the s-SNOM tip oscillates in tapping mode with frequency Ω, and different demodulation orders of the detector signal can be obtained. This allows to subtract undesirable background from the near-field scattering. Accordingly, to compare exactly with the near-field scattering signals obtained in s-SNOM, the amplitude and phase are also demodulated in the theoretical calculations. We will use in all our calculations a tapping frequency of $\Omega = 33$kHz, and a tapping amplitude of 25 nm, with the closest separation distance between tip and sample being 1 nm. We assume for the point dipole a polarizability corresponding to that of a sphere with a 25 nm radius. Typically, second and third order demodulation amplitude and phase signals are used in experiments. We will show calculations for the third order demodulation signals without loss of generality.

We will apply now this formalism to a situation where a sample layer of a material with a spectroscopic signature (i.e. a single molecular absorption band) is deposited on a substrate that interacts selfconsistently both with the sample layer and the near-field probing dipole (tip). p polarized light will be considered both for incident and detected light. Compared with static models previously used, this model includes additionally the retarded interaction of the dipole with the sample (more relevant as the point dipole is located further from the sample, and thick layers), and also the reflection of the backscattered radiation at the sample. The latter involves an extra reflection coefficient which can be relevant when analysing backscattering radiation of samples in highly reflecting substrates, as we will demonstrate in the following sections.

3. Signal in substrate-enhanced spectroscopy of a thin layer

It was already pointed out recently how a perfect mirror substrate or even a resonant tip-substrate interaction can enhance the near field contrast of nanoscale objects at a fixed infrared wavelength [14]. Following a similar approach, and motivated by experimental observations that will be presented in the next sections, we aim to enhance the spectral contrast and absolute s-SNOM amplitude signals of thin sample layers with the help of a convenient substrate.

3.1. PMMA layer on different substrates: SiO_2, Si, Au

We apply the formalism from the previous section to the infrared spectrum of a PMMA layer characterised by a dielectric function as shown in Fig. 2(a), on top of different substrate materials. In Figs. 2(b) and (c), we present calculations of the s-SNOM amplitude s_3 and phase φ_3

#90017 - $15.00 USD Received 21 Nov 2007; revised 16 Jan 2008; accepted 17 Jan 2008; published 22 Jan 2008

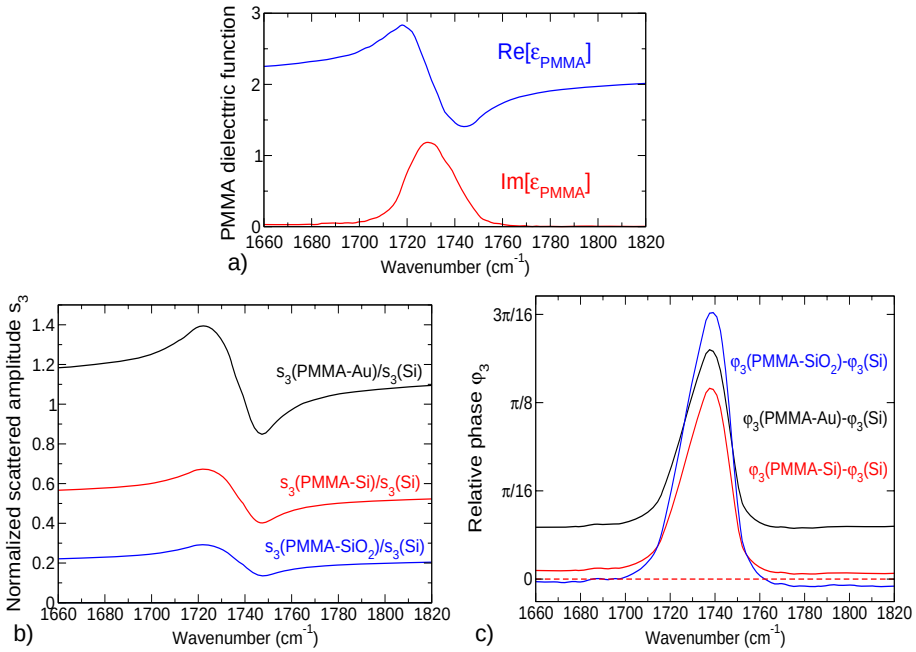

Fig. 2. (a) Real (Re[ε_{PMMA}]) and imaginary (Im[ε_{PMMA}]) parts of the PMMA dielectric function. Backscattering amplitude s_3 (b) and phase φ_3 (c) of a point dipole located on top of a 10 nm thick PMMA sample layer on different substrates. SiO_2 substrate in blue, Si in red, and Au in black. Demodulation order is $n = 3$. Amplitude is normalised to the value of a Si substrate in (b), and its phase value is used as a reference (red dashed line) in (c).

signals obtained from a 10 nm PMMA layer on SiO_2, Si, and Au respectively. The local dielectric functions are taken from experimental data [38]. Third order signals ($n = 3$) are calculated. As already shown previously [16, 17], the spectral response of a typical molecular absorption band shows the following signature in s-SNOM: the amplitude spectrum s_3 shows a derivative-like shape resembling roughly the real part of ε_{PMMA} or a reflection spectrum, while the phase spectrum φ_3 shows a peak at the frequency of the PMMA absorption band, roughly resembling the PMMA far-field absorption spectrum and is similar to the imaginary part of ε_{PMMA}. The asymmetric profile of the amplitude is a consequence of the phase interference of the electromagnetic fields between a narrow band (vibration) and a broad band (reflection) responses, analogous to the asymmetric Fano profiles given by the interaction between a discrete state and a continuum of states in quantum mechanics [39, 31]. Comparing the different substrates, the absolute amplitude signal s_3 of PMMA in the IR is enhanced by a factor of two for Si compared to SiO_2. This is in good agreement with the initial s-SNOM experiments of a PMMA film on a Si substrate [16], in which the s-SNOM spectra showed higher amplitude signals compared to what was theoretically expected for an infinite thick PMMA layer. Using an Au substrate for our calculations, the PMMA amplitude signal s_3 is again increased by another factor of two compared to the Si substrate. The phase signal φ_3 changes only slightly for the different substrates. The amplitude spectra in Fig. 2(b) show clearly that not only the absolute value of the signal is increased, but also the spectral feature (contrast) is scaled up. We will discuss this effect, which helps to improve the contrast in vibrational near-field IR spectroscopy, in more detail in section 4.1.

#90017 - $15.00 USD Received 21 Nov 2007; revised 16 Jan 2008; accepted 17 Jan 2008; published 22 Jan 2008

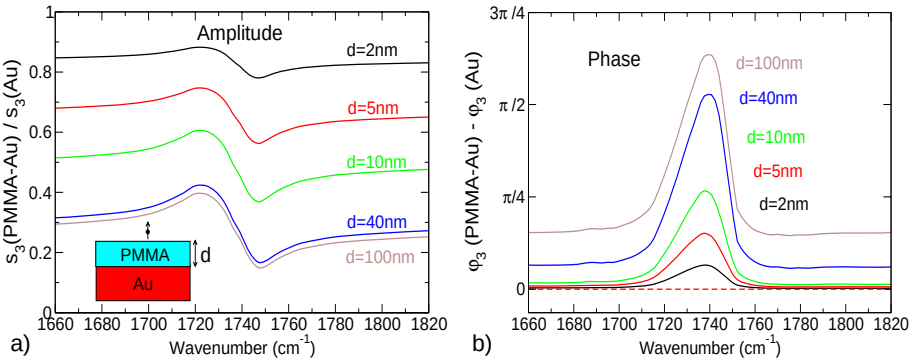

Fig. 3. Backscattering amplitude s_3 (a) and phase φ_3 (b) of a point dipole located above a PMMA sample layer of several different thicknesses deposited on top of a gold substrate. PMMA thicknesses are 2 nm (black), 5 nm (red), 10 nm (green), 40 nm (blue), and 100 nm (brown). 3^{rd} order demodulation is calculated, and the scattering amplitude is normalised to the scattering of a gold semiinfinite sample in (a). The phase for this reference case is plotted as a dashed line in (b).

3.2. Dependence on layer thickness

Another point of interest in substrate-enhanced near-field spectroscopy is the penetration depth of the tip near-field into the sample. Due to the strongly nonlinear distance-dependence of the near-field interaction between tip and sample, we expect the tip to interact differently with the substrate for sample layers of different thickness, giving rise to changes in the s-SNOM amplitude and phase signals and the related spectral contrast. To elucidate the effect of the sample layer thickness in the s-SNOM signals, and particularly the spectral contrast of the sample layer, we calculate normalized demodulated amplitude and phase signals, s_3 and φ_3, of the backscattered fields for different PMMA layers of different thickness on top of a gold substrate (see Fig. 3), which was considered the most appropriate material for spectral signal enhancement (see Fig. 2). Layers with a thickness of 100 nm, 40 nm, 10 nm, 5 nm, and 2 nm are considered. The amplitude signal s_3 increases by a factor of three from the thicker case (100 nm) to the thinner one (2 nm). This can be understood by a larger coupling of the tip near-field to the substrate. However, due to the presence of less quantity of absorbing (or "spectroscopically active") material, the contrast of the spectral amplitude signal s_3 diminishes as the PMMA layer gets thinner. This effect can be also observed in the phase φ_3 [Fig. 3(b)] where a smaller phase change occurs for thinner PMMA layers. Both the smaller phase change and the larger amplitude signals have already been observed experimentally in near-field amplitude and phase spectra of PMMA beads of heights ranging from 37 nm to 66 nm (see Fig. 4(c) in ref. [17]). We would like to note that monolayer sensitivity has already been reported in s-SNOM for both DNA layers [40], and lipids [10] when the layers were adsorbed on Au surfaces. However, as these experiments did not use interferometric detection, the reported spectra are difficult to interpret [24] and were assigned to vibrational absorption contrasts.

4. Spectral contrast in substrate-enhanced spectroscopy of a thin layer

We define the absolute spectral contrast Δs_3 as the difference between the maximum and the minimum of the spectral derivative-like amplitude of a vibrational resonance [see inset in Fig. 4(a)]. We then show in this section the effect of using different substrates to enhance the contrast of a thin sample layer with a spectral signature, and discuss the physical reason for this enhancement. We use both glass and gold as a substrate, and calculate the spectral contrast of

#90017 - $15.00 USD Received 21 Nov 2007; revised 16 Jan 2008; accepted 17 Jan 2008; published 22 Jan 2008

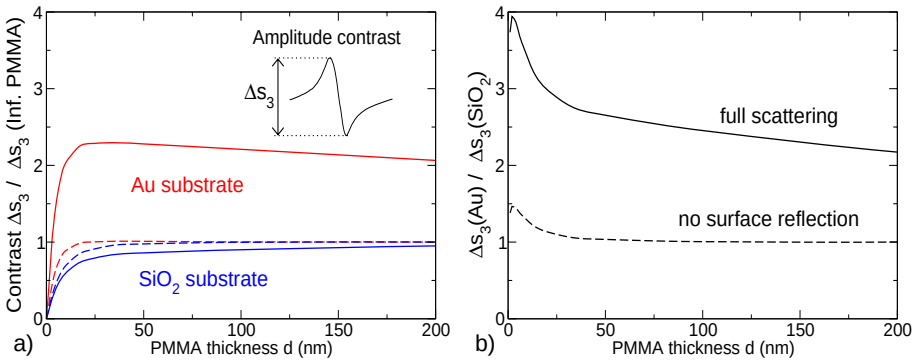

Fig. 4. (a) Contrast of a PMMA layer on a gold (red solid) and glass (blue solid) substrates as a function of the layer thickness, normalised to the contrast of an infinite PMMA substrate. Dashed lines represent the same calculation with the reflection of the incoming and outgoing radiation subtracted. The inset shows a scheme with the definition of spectroscopic contrast. (b) Ratio of contrasts $\Delta_{Au}/\Delta_{glass}$ as a function of the PMMA layer thickness. Solid line is the full calculation, and dotted lines denotes that the reflection of the incoming and outgoing radiation are subtracted.

a PMMA layer for continuously increasing layer thickness. The results are normalised to the contrast of an infinite thick sample of PMMA and plotted in Fig. 4(a). For thin PMMA sample layers (< 30 nm), we find that the contrast increases for both substrates as the PMMA thickness becomes larger, reaching saturation for thickness between 35 nm-50 nm. One can also observe that the contrast can be enhanced more than two times when the metallic mirror is used (red solid curve) with respect to a glass layer (blue solid curve). For thicker PMMA layers, the contrast is slowly attenuated towards the limit of the infinite PMMA layer. In Fig. 4(b) we plot with a solid line the ratio of the contrasts shown in Fig. 4(a) where we observe an increase of the efficiency of the metallic substrate down to PMMA layers of 2 nm. For this thin thickness, within the dipole approximation, the efficiency of the metallic substrate drops off.

4.1. Near-field interaction vs. surface reflection

We have shown that the use of a metallic substrate such as gold for infrared wavelengths enhances the spectroscopic amplitude signals of a vibrational fingerprint (PMMA signature). To elucidate whether this enhancement is a consequence of the near-field interaction, or rather a simple reflection-assisted mechanism, we calculate the same situation subtracting the reflection of the incoming radiation before hitting the tip (dipole), and also the reflection of the outgoing radiation of the dipole by the multilayered system. We represent the results as dashed lines in Fig. 4(a) and (b) together with the full calculations. It is obvious from the results in Fig. 4(b) that the main contribution to the two fold enhancement of a gold substrate with respect to the glass substrate comes from considering the reflection by the multilayered system. It is only for thin sample layers with $d < 30$ nm, i.e. in the close proximity between tip and substrate, that the near-field interaction contributes significantly to enhance the contrast Δs_3. In conclusion, the enhancement of both the absolute amplitude signal, and the corresponding spectral contrast Δs_3 is a consequence of the IR response of highly reflecting substrates. This response has a threefold effect in the scattering process: (i) the strong reflection of the incident radiation at the substrate enhances the tip illumination, (ii) the enhanced tip-substrate near-field interaction further increases the local field acting on very thin sample layers ($d < 25$ nm) owing to the selfconsistent multiple scattering within the tip-substrate gap responsible for the near-field, and

#90017 - $15.00 USD Received 21 Nov 2007; revised 16 Jan 2008; accepted 17 Jan 2008; published 22 Jan 2008

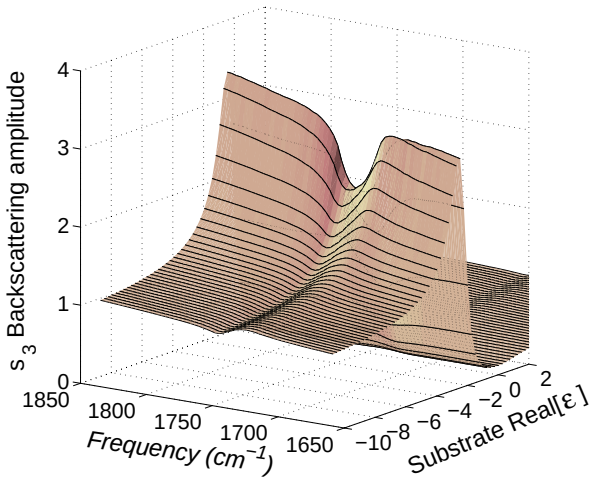

Fig. 5. s-SNOM amplitude spectra of a 2 nm PMMA layer on top of a substrate characterised by different values of the real part of its dielectric function, Re$\{\varepsilon_{subs}\}$. For values close to $\varepsilon_{subs} = -10 + 0.5i$ the PMMA spectra shows a typical derivative like line shape. Near $\varepsilon_{subs} = -1.66 + 0.5i$, signature interaction between tip and substrate becomes resonant and the PMMA signature changes to a single dip. 3^{rd} order demodulation is shown and the spectra are normalised to the signal of a substrate with $\varepsilon = -\infty$.

finally (iii) the reflection of the emitted radiation increases the backscattering. Note that the thickness of the thin sample layer where the near-field interaction occurs (ii) is comparable to the size of tip radius (≈ 25 nm).

5. Resonant tip-substrate interaction for spectroscopy of a thin layer

One of the situations which presents a promising enhancement potential for spectroscopic signal of thin layers relies on the use of resonant structures [41, 42, 43]. A resonant situation in s-SNOM can be achieved through the near-field interaction between the probing tip and a substrate supporting surface polaritons [44]. The near-field interaction becomes resonant for certain values of the sample's dielectric function, as demonstrated for a SiC surface [25]. In the following, we study the influence of resonant tip-substrate coupling on the s-SNOM spectral signal and contrast of a thin sample layer on a substrate.

5.1. Dependence on the dielectric properties of the substrate

We calculate the spectral amplitude signal for several constant dielectric values of the substrate ε_{subs} underneath a 2 nm PMMA sample layer, over the frequency range of the PMMA vibrational resonance. In Fig. 5 we vary the real part of the substrate's dielectric function $Re\{\varepsilon_{subs}\}$ from -10 to +2, (keeping the imaginary part as $Im\{\varepsilon\} = 0.5i$). The spectra are normalised to the amplitude signal of an infinite gold substrate with no sample layer. The tip-substrate coupling in the case of this thin sample layer exhibits a resonance at $Re\{\varepsilon_{subs}\} = -1.66$, which can be clearly observed from the signal maximum at a given frequency, e.g. at 1650 cm $^{-1}$. For a substrate with $Re\{\varepsilon_{subs}\} = -10$, we find the expected derivative-like signature for the PMMA layer with a moderate signal and contrast enhancement, similar to the case of a gold substrate ($Re\{\varepsilon_{subs}\} = -5000$) presented in previous sections. As the value of the substrate dielectric function gets closer to $Re\{\varepsilon_{subs}\} = -1.66$, the s-SNOM signal s_3 shows a resonant

#90017 - $15.00 USD Received 21 Nov 2007; revised 16 Jan 2008; accepted 17 Jan 2008; published 22 Jan 2008

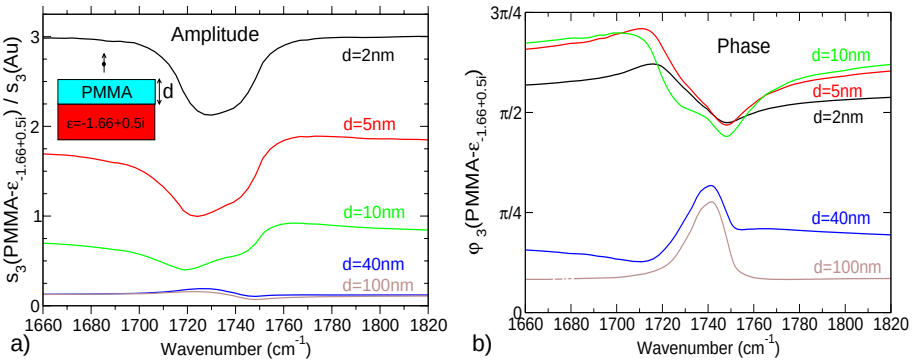

Fig. 6. Backscattering amplitude s_3 (a) and phase φ_3 (b) of a point dipole located on top of a PMMA sample layer of different thickness deposited on a substrate producing a "quasi-resonant" tip-substrate interaction ($\varepsilon_{subs} = -1.66 + 0.5i$). Thicknesses of the PMMA sample layer are 2 nm (black), 5 nm (red), 10 nm (green), 40 nm (blue), and 100 nm (brown). 3^{rd} order demodulation is calculated, and the scattering amplitude is normalised to the scattering of a semiinfinite gold sample in (a). Strong line shape change is observed for different sample layer thicknesses.

tip-substrate coupling. This resonant situation produces an increase in the s-SNOM signal of more than one order of magnitude, and an increase of the contrast of the spectral features of the PMMA layer. Interestingly, the line shape of the spectrum also changes when approaching near resonance from derivative-like to a dip. This effect is due to the electromagnetic interaction between the vibrational resonance of the sample layer and the tip-substrate resonance, producing a Fano-like antiresonance (dip in the spectrum) due to the interference of fields in opposite phases. [31, 45].

As the substrate response ε_{subs} departs from resonance (real part of the substrate dielectric function between -1.66 and 2), the PMMA fingerprint is recovered with much smaller amplitude and contrast. Although the spectral shape of the PMMA fingerprint is modified near resonance, the s-SNOM signal from a thin sample layer (monolayer for example) is increased dramatically by the resonant tip-substrate coupling, allowing for resonant infrared near-field spectroscopy when the tip-substrate interaction is conveniently tuned.

In a realistic situation for a substrate, the dielectric response will show a certain dispersion. The spectral line could be obtained in that case, by tracing for each frequency in Fig. 5 the different values of the substrate dielectric function. Independently of the actual dispersion of the substrate, Fig. 5 shows that by going through the tip-substrate resonance ($Re\{\varepsilon_{subs}\} = -1.66$), an enhanced spectral contrast can be obtained.

5.2. Dependence on the thickness of the sample layer

For a layered system, the condition of resonant tip-substrate interaction will depend on the tip-substrate distance [26] and also on the dielectric value of the sample layer. If we select the material of our sample layer (PMMA), and we also fix the dielectric value of the substrate supporting the sample layer, the resonant condition for the s-SNOM signal will depend on the tip-substrate separation distance, mainly determined by the thickness of the PMMA sample layer. We therefore change the resonant condition when we change the thickness of the sample layer. For PMMA sample layers, the values for the dielectric

function of the substrate ε_{subs} that generates resonant tip-substrate coupling, vary from $Re\{\varepsilon_{subs}\} = -1.66$ for a thickness of 2 nm, down to $Re\{\varepsilon_{subs}\} = -2.07$ for a thickness of

#90017 - $15.00 USD Received 21 Nov 2007; revised 16 Jan 2008; accepted 17 Jan 2008; published 22 Jan 2008

100 nm. For simplicity, we select a fixed constant value $\varepsilon_{subs} = -1.66 + 0.5i$ for all the PMMA sample layer thicknesses studied, even though this value makes the tip-substrate coupling exactly resonant only for a 2 nm PMMA layer. We present the results in Figs. 6(a) and (b). For very thin PMMA sample layers, the s-SNOM signal s_3 is enhanced by more than one order of magnitude. Similar to Fig. 5, the spectral signature changes from derivative-like pattern for thick layers (d=40 nm and d=100 nm) to a pronounced dip in the spectrum for thinner layers (d=2 nm and d=5 nm), where the resonant tip-substrate coupling is strongest. Note that for thick layers, the tip-substrate coupling is negligible, recovering the standard signature of PMMA. The amplitude signal drops off in this latter case (blue and brown lines), getting values similar to those obtained for highly reflecting substrates. Similar effects of line shape change can be observed in the phase [Fig. 6(b)], going from a standard peak for thick PMMA samples to a derivative-like shape of larger contrast for thin PMMA sample layers. Even though the change of lineshape needs to be correctly interpreted, the huge amplitude signals obtained for thin sample layers [see Fig. 6(a)], and the distinctive spectral signature (though different than the original one) might be applied for enhanced spectroscopy of single molecular monolayers.

6. Experimental results

To demonstrate experimentally the enhancing effect of a substrate on the contrast in vibrational spectroscopy with a s-SNOM, we measured the spectral response of a thin polymethylmethacrylate(PMMA) layer on both Au and Si substrates. The measurements were performed with an s-SNOM setup based on a home built tapping-mode Atomic Force Microscope (AFM) with a Cassegrain objective (NA=0.55) added to illuminate the tip with light from a mid-infrared line-tuneable CO-laser [16, 18]. The scattered light is detected interferometrically with a liquid-nitrogen cooled MCT-detector. The Pt-coated tip (Mikromasch) oscillates at its resonance frequency Ω ($\approx$ 35 kHz) with a tapping amplitude of 50 nm, while the sample is scanned. For background suppression a pseudoheterodyne interferometric detection scheme as described in Ref. [34] is used. The infrared amplitude s_n and phase signals φ_n are evaluated at the frequency $n\Omega$, with $n = 3$ in the following experiments. For a fixed wavelength setting of the laser, the topography, the infrared amplitude s_3 and phase φ_3 image are recorded simultaneously.

The sample used for this spectroscopic study consists of a Si wafer with a structured, 20 nm thick Au film patterned by colloidal lithography [46]. After preparation of the Au film, a layer of PMMA was spincoated from solution on the sample to obtain a film thickness of about 50 nm on the Si and about 40 nm on the Au surfaces [Fig. 7(b)]. For height measurements, and as a reference for the spectroscopic signal in s-SNOM, both the Au and the polymer are partly removed by scratching with a needle to reveal the Si substrate. The topography image [(Fig. 7(a)] shows the bare Si substrate on the left and an elevated PMMA film covering some Au islands on the right side of the image. Infrared amplitude images at 2 different wavelength settings of the CO-laser are shown in Fig. 7(c,d). Both yield the highest amplitude on the Si substrate, the PMMA-covered Au islands appear slightly darker and the PMMA film has the lowest infrared amplitude s_3. The contrasts between the response s_3 of the bare Si and Si covered with PMMA changes noticeably at the different wavelengths, indicating the vibrational absorption band of PMMA around 1728 cm^{-1}. This feature appears in the spectral evaluation of areas marked with A, B, C in Fig. 7(d) from images taken at different wavelengths, normalized to the amplitude averaged over the marked area on the Si substrate. The results [Fig. 7(e)] show the typical spectral signature for PMMA in a scattering-type near field optical microscope [16], as discussed earlier on: The amplitude roughly follows the real part of the PMMAs dielectric function $\varepsilon(\omega)$, with a maximum slightly below and a minimum above the resonance frequency of the Lorentz-oscillator describing the infrared response of PMMA.

A closer look at the spectra taken at different positions reveals that the scattered amplitude s_3

#90017 - $15.00 USD Received 21 Nov 2007; revised 16 Jan 2008; accepted 17 Jan 2008; published 22 Jan 2008

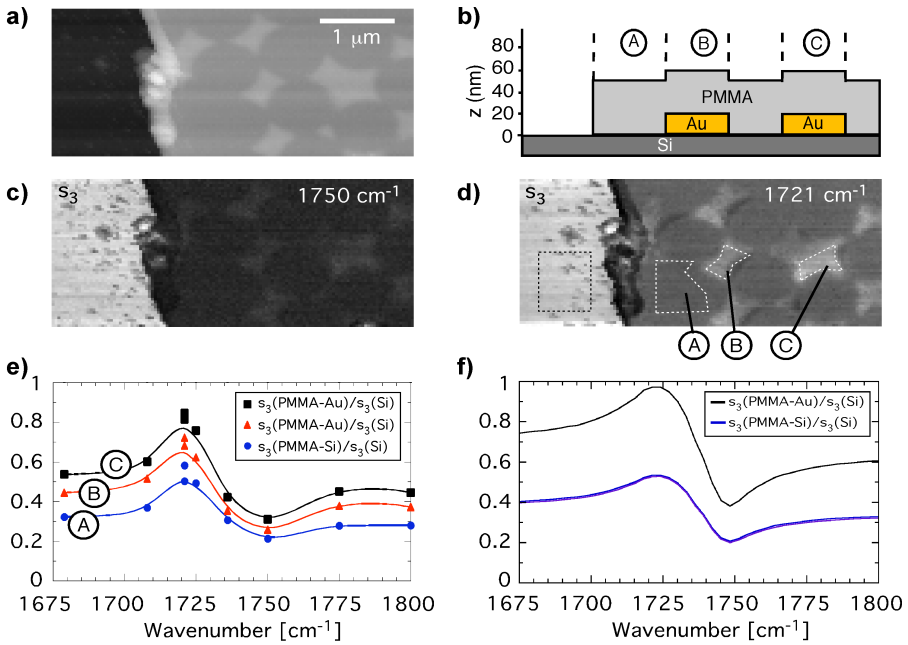

Fig. 7. Topography (a), schematic cross-section (b) and normalized infrared s-SNOM amplitude images (c-d) of a sample consisting of Au island on Si, partly covered with a thin PMMA film. Experimental s-SNOM spectra (e) are obtained by extracting infrared amplitude values s_3 averaging over the areas (A) PMMA on Si, (B) PMMA on a Au island and (C) PMMA on another Au island, and normalizing them to the averaged amplitude value s_3 on Si (area marked with dark dashed line in (d)). The solid lines in the spectra (e) are a smoothed connection between the data points and serve as a guide to the eye. The corresponding theoretical spectra are shown in (f). Both scattering amplitude as well as contrasts are enhanced on Au compared to the Si substrate.

is higher for the PMMA on Au, compared to PMMA on Si, throughout the whole spectrum. As predicted in Sections 3.1, the presence of a highly reflecting substrate clearly enhances the scattered amplitude. Slight changes of the PMMA thickness on the Au substrate (40 nm) compared to the Si substrate (50 nm) can be discarded as the reason for the enhancement. In Fig. 3(a) we already showed that the difference between a 40 nm and a 100 nm thick layer of PMMA is much smaller than the experimental accuracy. We additionally performed calculations considering the PMMA thickness in the experiment on both Au and Si substrates [Fig. 7(f)]. We observe that a thickness variation on Si from 40 nm to 50 nm does not alter the scattered amplitude signal s_3 significantly (less than 3% difference). The calculated spectra predict maximum (minimum) amplitudes of 0.95 (0.4) on Au, and 0.5 (0.2) on Si, close to the experimentally observed values of 0.8 (0.3) on Au, and 0.5 (0.2) on Si. The qualitative agreement is evident, and the quantitative differences on Au can be due to the finite size of the Au islands. More important, the spectral contrast (again defined by the difference between the minimum and maximum in the spectrum) is increased on Au almost exactly as predicted, from 0.3 to 0.5 of the signal obtained on Si. This confirms the predictions of section 3, Fig. 2(b). In other words, we have proven that the presence of the highly reflecting substrate does not only add a constant signal offset (constant value to the amplitude signal s_3 along the whole spectrum), but is also able to strengthen the spectral contrast Δs_3, thereby increasing the s-SNOMs chemical sensitivity.

We also note that some Au islands appear brighter than others. For example, the spectrum on

#90017 - $15.00 USD Received 21 Nov 2007; revised 16 Jan 2008; accepted 17 Jan 2008; published 22 Jan 2008

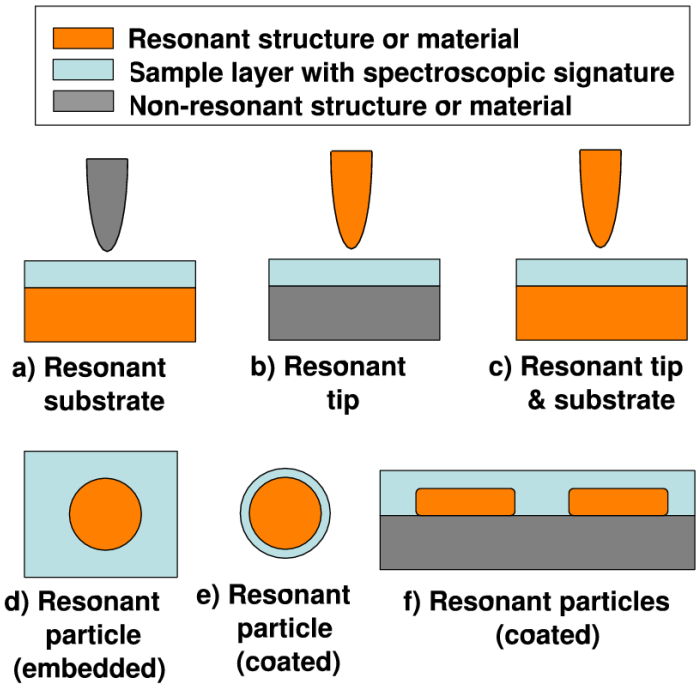

Fig. 8. Schematics of different situations that can host substrate-enhanced near field infrared scattering efficiently when a resonant structure is located nearby: (a) subsurface resonant substrate, (b) resonant tip, (c) Substrate and tip resonant, (d) a resonant particle embedded in a layer with signature, (e) a resonant particle coated by a layer with a signature, and (f) resonant particles buried by a sample layer under study.

island C yields higher scattering amplitude compared to on island B. These enhanced signals result from a stronger near-field interaction. Small metallic particles, similar to ours in shape and arrangement, are known to exhibit localized plasmon resonance, which can also occur at mid-infrared frequencies [47]. Far-field FT-IR reflection spectra of the same sample, albeit averaged over larger areas, revealed indeed a broad peak centered around 2400 cm $^{-1}$. We can therefore not exclude that in the experiment some of the Au islands might have been close to a plasmon resonance. As pointed out in the previous section, the combination of substrate-enhanced near-field spectroscopy along with resonant structures or tip-substrate interaction promises even higher enhancement factors than a reflecting surface can offer. Definitely more experimental and theoretical work will be needed to understand this exciting topic, since overlapping resonances of molecules and plasmonic structures will eventually change spectral shape and positions, as already mentioned in the sections before.

7. Surface-enhanced Infrared scattering (SEIRS)

We would like to conclude this contribution by extending the concept of resonant substrate-enhanced near-field infrared scattering to general situations where a resonant environment can be designed. In the particular case of s-SNOM, we have studied here the effect of resonant tip-substrate coupling [Fig. 8(a)], but a similar effect in the enhancement of the spectral signal and contrast could be expected with the use of a resonant tip [Fig. 8(b)] that could be brought close to the sample layer. An ultimate example of a resonant situation could be achieved when

#90017 - $15.00 USD Received 21 Nov 2007; revised 16 Jan 2008; accepted 17 Jan 2008; published 22 Jan 2008

both tip and substrate are resonant [Fig. 8(c)]. An analogous situation can be obtained if a material with a vibrational signature in the infrared could surround a resonant structure (matrix sample embedding a resonant particle), or if just a thin sample layer of the material surrounds the resonant particle [Fig. 8(d) and (e)]. Several variations of this resonant behavior can be conceived [Fig. 8(f)], and some approaches based in a similar idea have been implemented by some groups to perform molecular spectroscopy in configurations where the vibrational fingerprint interacts with various resonant situations (infrared absorption on hole arrays [42], on dielectric nanoparticles [48], or on infrared nanoantennas [49]). The main feature to point out - in all those resonant cases - is the strong electromagnetic interaction between the vibrational excitation and the near field of the resonant structure, similar to our case of a sample layer in a resonant tip-substrate interaction in s-SNOM. Finally, we note that in all the cases described, not only the signal can be enhanced, but also a change of the spectral signature of the sample layer can be expected, both in amplitude and phase.

8. Conclusions

We have presented a formalism that allows for the calculation of the amplitude and phase signals in s-SNOM of a sample layer deposited on a substrate. The role of the substrate has been studied with use of this formalism. We find that highly reflecting materials such as metals in the infrared enhance the spectroscopic signal of a thin sample layer, based mainly on the effect of reflection of the substrate. However, for sample layers thinner than the tip radius, the near-field interaction between tip and substrate plays a role and larger contrast is obtained. Experimental confirmation of this features has been obtained for PMMA layers on islands of gold. We further predict that the use of resonant tip-sample interaction can lead to huge enhancement of both the amplitude signal and the spectral signature (contrast). Our results show that the use of a resonant tip-substrate coupling could improve the spectral contrast of a PMMA layer in more than one order of magnitude. Even though this effect changes the spectral signature, it helps to significantly improve the sensitivity (signal strength and spectral contrast) of s-SNOM for probing thin sample layers or even small particles [14, 15].

Acknowledgements

We wish to acknowledge discussions with N. Ocelic and F. Keilmann, and financial support from the Department of Industry of the Basque Country (ETORTEK project NANOTRON), from Gipuzkoa Foru Aldundia (nanoGUNE), from the Spanish MEC (NAN2004-08843-C05-05 and MAT2007-66050), from BMBF grant no. 03N8705, and from the Bavarian California Technology Center (BaCaTec). T.T. was supported by a fellowship within the Postdoc-Programme of the German Academic Exchange Service (DAAD).

Appendix

We write in this Appendix the expressions of the reflection and transmission coefficients of the different layers, used to calculate the reflection of the external field E^0 acting on the dipole, as well as the self-interaction G of the dipole. The reflection coefficients r^s_{ij} and r^p_{ij} stand for the amplitude reflection back into medium i by medium j, for s and p polarized light respectively:

$$r^s_{ij} = \frac{k^i_z - k^j_z}{k^i_z + k^j_z} \tag{18}$$

and

$$r^p_{ij} = \frac{\varepsilon_j k^i_z - \varepsilon_i k^j_z}{\varepsilon_j k^i_z + \varepsilon_i k^j_z}. \tag{19}$$

#90017 - $15.00 USD Received 21 Nov 2007; revised 16 Jan 2008; accepted 17 Jan 2008; published 22 Jan 2008

Analogously, the transmission coefficients t_{ij}^s and t_{ij}^p stand for amplitude transmission from medium i into medium j for the different polarizations s and p:

$$t_{ij}^s = \frac{2k_z^i}{k_z^i\varepsilon_j + k_z^j\varepsilon_i}, \tag{20}$$

and

$$t_{ij}^p = \frac{2k_z^i\sqrt{\varepsilon_i\varepsilon_j}}{k_z^i\varepsilon_j + k_z^j\varepsilon_i}, \tag{21}$$

These expressions are referred to reflections and transmissions at individual interfaces between 2 different layers. We can express the total reflection R of the multilayer system as a function of the individual reflections and transmissions. We obtain for p polarization, with $R = R_{12}^p$:

$$R_{12}^p = r_{12}^p + \frac{t_{12}^p t_{21}^p e^{i2k_z^{(2)}d}\left[r_{23}^p + \frac{t_{23}^p r_{34}^p t_{32}^p e^{i2k_z^{(3)}z'}}{1-r_{32}^p r_{34}^p e^{i2k_z^{(3)}z'}}\right]}{1 - r_{21}^p r_{23}^p e^{i2k_z^{(2)}d}}. \tag{22}$$

The same expression stands for s polarization. In that case, $R = R_{12}^s$ is expressed as a function of the corresponding transmission t_{ij}^s and reflection r_{ij}^s coefficients.

#90017 - $15.00 USD Received 21 Nov 2007; revised 16 Jan 2008; accepted 17 Jan 2008; published 22 Jan 2008